The ratio of the free n-p cross section, as calculated and as measured, is listed in Table VIII. The effect of the energy threshold of this experiment was included in the calculation. Note that the measured ratio, typically 0.65 ± 0.04, is significantly smaller than the calculated ratio, typically 0.76. Note also that the measured ratio is quite angle-independent (except at the largest lab angle, 50°), as is seen by the constancy of R_M within a data period, where the smaller error, $\delta R_M(R)$, applies.

The difference between polarization parameters for free n-p scattering and for the reaction $n+d\rightarrow p+2n$, as measured and as calculated, are listed in Table X. The measured difference is small, consistent with the calculated difference, but also consistent with zero.

ACKNOWLEDGMENTS

We gratefully acknowledge the participation of Dr. N. W. Reay in the early stages of this experiment. We thank Professor Breit for sending us extensive results of his phase-shift analyses.

PHYSICAL REVIEW VOLUME 167, NUMBER 5 25 MARCH 1968

Forward π^-p Charge-Exchange Scattering between 561 and 2106 MeV/c*†‡

WINTHROP S. RISK
Princeton University, Princeton, New Jersey
(Received 11 August 1967)

Final results are presented from a spark-chamber experiment performed at the Princeton-Pennsylvania Accelerator to measure the differential cross section near 0° for the reaction $\pi^-p\rightarrow\pi^0n$. The data are extrapolated to 0° and the results of the extrapolation are compared with the results of other experiments and with dispersion relation predictions. The values of the forward-scattering amplitude for the fifteen values of incident π^- momentum at which measurements were made are as follows: (p (MeV/c), $(d\sigma/d\Omega)_0$° (mb/sr)): (561, 3.28), (636, 2.95), (687, 3.38), (750, 2.48), (802, 1.33), (930, 2.42), (1005, 3.15), (1030, 3.43), (1077, 1.70), (1134, 1.04), (1434, 0.31), (1579, 0.56), (1711, 0.73), (1914, 0.87), (2106, 0.56). The combined statistical and systematic uncertainties in these values is about ±9%. A description of the apparatus, a discussion of the methods of analysis, and a discussion of the errors contributing to the uncertainties in the above results are included in the text.

I. INTRODUCTION

THIS experiment was performed at the Princeton-Pennsylvania Accelerator (P.P.A.) in the fall of 1964 at which time the available measurements of the π^-p charge-exchange forward amplitude $[d\sigma/d\Omega(0°)]$ were those below 550 MeV/c [1] and those of Saclay [2] in the interval 900–2000 MeV/c. The measurements below 550 MeV/c offered convincing experimental proof of the pion-nucleon dispersion relations developed by Goldberger *et al.*[3] These relations, involving no assumptions about the dynamics of the pion-nucleon interaction, express $d\sigma/d\Omega(0°)$ in terms of integrals over the elastic total cross sections $\sigma(\pi^\pm p\rightarrow\pi^\pm p)$. The Saclay measurements showed generally good agreement with the dispersion relations, but were systematically high around 1500 MeV/c.

There are now available measurements of the total angular distributions for $\pi^-p\rightarrow\pi^0n$ [4] in the energy region covered by this experiment and a number of recent measurements of $\sigma(\pi^\pm p\rightarrow\pi^\pm p)$.[5] Dispersion calculations of $d\sigma/d\Omega(0°)$ have been published beginning with the work of Cronin,[6] but the most detailed calculations and comparisons with the experimental data have been done by Höhler *et al.*[7] Reference 7 also gives a fairly complete summary of the experimental and theoretical work to date.

As these additional results become available, it was

* Work supported by the U. S. Office of Naval Research under Contract No. AT(30-1)3406.

† Based in part on a thesis submitted in partial fulfillment of the requirements for the degree of Doctor of Philosophy in Physics, Princeton University.

‡ This work made use of computer facilities supported in part by National Science Foundation Grant No. NSF-GP 579.

[1] V. G. Zinov and S. M. Korenchenko, Zh. Eksperim. i Teor. Fiz. **36**, 618 (1959) [English transl.: Soviet Phys.—JETP **9**, 429 (1959)]; J. C. Caris, R. W. Kenney, V. Perez-Mendez, V. A. Perkins, Phys. Rev. **121**, 893 (1961).

[2] P. Borgeaud, C. Bruneton, Y. Ducros, P. Falk-Vairant, O. Guisan, J. Movchet, P. Sonderegger, A. Stirling, M. Yvert, A. Tran Ha, and S. D. Warshaw, Phys. Letters **10**, 134 (1964).

[3] M. L. Goldberger, H. Miyazawa, R. Oehme, Phys. Rev. **99**, 986 (1955); M. L. Goldberger, *ibid.* **99**, 979 (1955).

[4] L. Guerriero, Proc. Roy. Soc. (London) **A289**, 471 (1966); C. B. Chiu *et al.*, Phys. Rev. **156**, 1415 (1967). The author wishes to thank Professor R. E. Lanou of Brown University for providing more recent results than those of Guerriero.

[5] W. Galbraith, E. W. Jenkins, T. F. Kycia, B. A. Leontic, R. H. Phillips, A. L. Read, and R. Rubenstein, Phys. Rev. **138**, B913 (1965); T. J. Devlin, J. Solomon, and G. Bertsch, Phys. Rev. Letters **14**, 1031 (1965); B. Amblard, P. Borgeaus, Y. Dueros, P. Falk-Vairant, O. Guisan, W. Laskar, P. Sonderegger, A. Stirling, M. Yvert, A. Tran Ha, and S. D. Warshaw, Phys. Letters **10**, 138 (1964).

[6] J. W. Cronin, Phys. Rev. **118**, 824 (1960).

[7] G. Höhler, J. Baacke, and R. Strauss, Phys. Letters **21**, 223 (1966); G. Höhler, J. Baacke, J. Giesecke, and N. Novko, Proc. Roy. Soc. (London) **A289**, 500 (1966).

hoped that the present experiment with better statistics and better resolution could give more definite conclusions than the previous work. In particular, with the improved measurements of $\sigma(\pi^{\pm}p \rightarrow \pi^{\pm}p)$ used in the dispersion calculations, the Saclay results agree quite well around 1500 MeV/c but are now systematically low around the resonance at 1000 MeV/c. The total angular-distribution measurements give values of the forward amplitude generally consistent with the dispersion relations, but now these measurements are systematically high around 1500 MeV/c.

II. DESCRIPTION OF THE EXPERIMENT

A. π^- Beam

A triple-focused negative beam was constructed at 13° relative to the internal proton beam of the Princeton-Pennsylvania Accelerator (P.P.A.). Three-BeV protons striking an internal Pt target $1\frac{1}{2}$ in. long $\times\frac{1}{2}$ in. high$\times\frac{1}{4}$ in. thick produce π^- and e^-. Decaying π^- result in a μ^- component in the beam as well. The π^- flux at the experimental apparatus was as high as 500 particles/pulse at 20 pulses/sec with a momentum bite of $\pm 0.75\%$. The pulse length was 1 msec and had an internal structure of 1-nsec-wide bunches 33 nsec apart, due to the rf bunching of the internal proton beam. The momentum bite was fixed at the first focus of the beam using an 18-in.-long iron collimator with variable aperture. A $\frac{1}{4}$-in. aperture gave the 0.75% momentum bite. Above 1400 MeV/c, a $\frac{1}{2}$-in. aperture was used to give $\pm 1.25\%$. Determination of the momentum dispersion at the collimator and of the required quadrupole magnet fields was done initially with a computer program OPTIK[8] and then refined using wire orbit techniques. A wire orbit calibration of momentum versus bending magnet current was done for each bending magnet (B.M.). The wire orbit results were reproducible to about 0.1% and were sensitive enough to detect 0.3% hysteresis effects in the bending magnets. These effects were compensated by running the magnet to saturation before reducing the current to the desired value. The π^- accepted by the experiment were defined by four scintillation counters ($T_1T_2T_3T_4$, Fig. 1). The counters (T_3T_4) were 2 in. in diameter to limit the beam-spot size. A spark chamber[9] before T_3T_4 was used to get a measurement of the incident π^- trajectory. A flask of liquid H_2, $3\frac{1}{2}$ in. in diameter$\times 2\frac{1}{4}$ in. long after (T_3T_4), was the proton target.[9] By reconstructing tracks in the beam chamber, the beam spot at the H_2 target using ($T_1T_2T_3T_4$) was determined to be 2 in. high$\times 1\frac{1}{4}$ in. wide at 575 MeV/c decreasing to $1\frac{1}{2}$ in. $\times\frac{3}{4}$ in. above 1500 MeV/c. Before each run at a different momentum, a counter $\frac{1}{4}$ in. wide$\times 2$ in. high (T_4') replaced T_4 and the current in B.M. I was adjusted to maximize the count rate in T_4'. The rate in T_4' versus current of B.M. I was quite sharply peaked, with a full width at half-maximum approximately the size of the momentum bite. Relative to the wire orbit calibration, this maximization procedure gave a systematic shift of about 1% downward in the momentum defined by B.M. I. Time-of-flight measurements on π's, p's, and d's, using a positive beam obtained by reversing the B.M. fields, were done at several momenta between 600 and 2200 MeV/c. These results agreed with the wire orbit results to better than 2%, but systematic effects were observed which will be discussed in Sec. IV C. The μ and e contamination of the beam was measured using a gas (SF_6) Čerenkov counter similar to the one in Ref. 10 and varied from 25% at 575 MeV/c to less than 3% above 1500 MeV/c. Further discussion of these measurements is given in Sec. IV D.

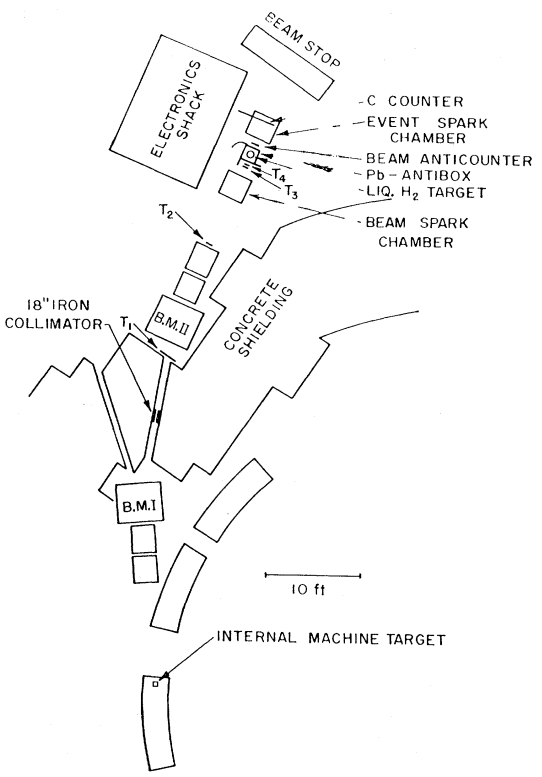

FIG. 1. Schematic diagram of experimental layout.

B. Detection of the Reaction $\pi^-p \rightarrow \pi^0n$

The π^0 is detected using the γ rays of its principal decay mode ($\pi^0 \rightarrow 2\gamma$; 99%).

1. Event Spark Chamber

Downstream from the liquid H_2 target was a spark chamber with $\frac{1}{4}$-in. lead plates for converting ($\gamma \rightarrow e^+e^-$) and thereby detecting the π^0 γ rays. This chamber was

[8] T. J. Devlin, University of California Radiation Laboratory Report No. UCRL 9727, 1961 (unpublished).

[9] Winthrop S. Risk, Ph.D. thesis Princeton University, E.P.L. Report No. 38, 1965 (unpublished).

[10] V. Perez-Mendez and J. H. Atkinson, University of California Radiation Laboratory Report No. UCRL-8750, 1958 (unpublished).

contained inside a vacuum-tight box 30 in.×30 in.×9 in. with $\frac{3}{4}$-in.-thick aluminum walls. Each converter was followed by two $\frac{3}{8}$-in. gaps. The spark-chamber plates were 27 in. square and were constructed by stretching 1-mil-thick aluminum foil on aluminum frames. The first converter was attached directly to the inside wall of the vacuum box, while the second converter was mounted inside the central spark-chamber plate. 90° stereo views looking down each gap were obtained on a single frame of 35-mm film by using plano-convex Lucite lenses and an appropriate mirror system. A frame number was also in view to permit correlation of the event and beam-chamber photographs. Fiducial marks whose positions within the chamber were accurately known were made to permit reconstruction of the tracks from film measurements. Because of the difficulty of adequately illuminating these marks for every frame, grids inscribed on Lucite plates and illuminated by flash tubes were mounted over the lenses outside the chamber box. A scintillation counter C, $\frac{1}{2}$ in.×24 in.×24 in. with a light pipe extending through a vacuum seal in the side of the chamber box, was mounted immediately after the last spark-chamber plate, inside the box. Photomultiplier tubes were attached to the light pipe outside the box. The chamber was evacuated, then filled with a 90-10 commercial neon-helium gas mixture and sealed. During a run, the gas would have to be changed about every two days.

2. Counter Logic

Referring to Fig. 1, in addition to the telescope $T=(T_1T_2T_3T_4)$ and the counter C, an array of $\frac{1}{2}$ in. thick scintillators forming a box 14 in. square at its base and 24 in. high was constructed around the hydrogen-target vacuum tank. Inside the scintillator box was another box made of 0.4-in.-thick Pb plates to convert nonforward γ rays from inelastic reactions, e.g. $(\pi^- p \rightarrow 2\pi^0 n)$. Both the scintillator and Pb forming the upstream side of the box had a 4-in.-diam entrance hole for the beam. For the exiting γ rays, there was a 9-in.-square hole in the downstream side of the Pb box. In addition, a 3-in.-diam hole in the downstream scintillator was covered by a 6-in.×6-in.×$\frac{1}{8}$-in. counter to maintain full rejection of the high flux of beam particles and forward-scattered charged particles. The top of the box was open for plumbing connections to the H_2 target. Adding the Pb and scintillator on the sides, back and bottom, to the front Pb-anticoincidence counter pair reduced the trigger rate by a factor of 4–5 depending on momentum of the π^-. The logic $T\bar{A}C$ then implied that a charged particle entered the target, no charged particle came out, and a charged particle materialized in the event chamber. Completion of the logic triggered the spark chambers, the fiducial lights and frame number, advanced the frame number and the camera frame, and turned on a 50-msec deadtime gate.

3. Geometrical Considerations of the Apparatus

For a given spark-chamber size (active area 26 in. ×26 in.), the length of the hydrogen target (ΔL) and the distance from hydrogen target to event chamber (L) are restricted by the desired event rate, and by the desired resolution and efficiency of the apparatus. The following factors must be taken into account in determining L and ΔL.

(a) Since the interaction point of the π^- along the length of the hydrogen target is unknown, and since multiple scattering of the showers in the event chamber does not allow them to give the γ-ray directions from the target, it is necessary to pick a point (the center) along the target and use the γ-ray conversion points in the converters to define the γ-ray trajectories. Given the γ-ray and the π^- trajectories, the π^0 direction can be determined. The accuracy of the determination depends on $(\Delta L/L)$, which should be as small as possible.

(b) ΔL should be large, however, to maximize the rate as well as to minimize the target-empty effect. (Events produced in the windows of the hydrogen target and in the counters nearest the target.)

(c) Consistent with (b), L should be large enough to maximize the statistics in the forward direction and thereby obtain a better extrapolation to zero degrees. However, L cannot be so large that the solid angle accepted by the apparatus becomes comparable to the over-all resolution of the experiment, which is governed also by the measuring accuracy and the momentum bite of the π^- beam.

(d) The momentum bite must be large to maximize the rate, but small relative to the rate of change of the cross section versus momentum. In the regions around 700 and 1000 MeV/c, this requirement limits $\Delta p/p$ to $<2\%$.

(e) The two γ's which are observed from the π^0 decay have a distribution of opening angles beginning with a minimum angle. The requirement that we maintain a reasonable efficiency for an appreciable fraction of γ opening angles at the largest π^0 scattering angle determined by (c) essentially fixes L. Consequently, ΔL is fixed, while $\Delta p/p$ is fixed by (d).

For the values L, ΔL, and $\Delta p/p$ used in the experiment, Table I, ΔL was the main factor affecting the accuracy of the determination of the π^0 direction. The uncertainty in measuring the shower positions gave a smaller but noticeable effect, while the effect due to $\Delta p/p$ was negligible.

In the analysis events were accepted if they had a geometrical detection efficiency $>10\%$. The smallest value of $\cos\theta_{\pi^0}$ (θ_{π^0} is the π^0 direction relative to the π^- trajectory) and the fraction of events included within the largest γ opening angle for which this condition is satisfied is given in Cols. 4 and 5 of Table I. The resolution in $\cos\theta_{\pi^0}$ was determined to be $\sim\pm 0.003$ in the

TABLE I. Summary of some of the experimental parameters and various experimental errors. Col. 1, incident π^- momentum. Col. 2, distance in in. of hydrogen target to event chamber. Col. 3, percent momentum bite of π^- beam. Col. 4, minimum $\cos\theta_{\pi^0}$ below which no events have detection efficiency greater than 10%. Col. 5, fraction of all elastic events at $\cos\theta_{\pi^0}{}^{\min}$ which have detection efficiency greater than 10%. Col. 6, No. of real elastic events accepted for analysis. Col. 7, percent inelastics and uncertainty. Col. 8, ±% uncertainty due to factors in Sec. IV. Col. 9, ±% uncertainty due to factors in Sec. VI.

1	2	3	4	5	6	7	8	9
561 No. 1[a]	21.4	0.75	0.94	0.7	1660	9.5±3.5	6	5.5
636	21.4	0.75	0.94	0.7	1180	21.1±5.6	6.5	3.5
687	21.4	0.75	0.94	0.7	2590	17.3±4.7	5.5	4
750	21.4	0.75	0.94	0.8	1480	16.5±4.1	5	6.5
802	21.4	0.75	0.94	0.8	1150	23.0±5.3	6.5	4
930	35.6	0.75	0.97	0.7	1200	16.9±3.7	4.5	3.5
1005	35.6	0.75	0.97	0.7	1270	19.1±5.3	6	4.5
1030	35.6	0.75	0.97	0.7	1670	17.0±4.4	5.5	3.5
1077	21.4	0.75	0.93	>0.9	1370	13.5±3.8	4.5	3.5
1134	35.6	0.75	0.97	0.8	1280	25.3±5.5	6	4
1434	21.4	1.25	0.93	>0.9	2530	21.5±4.6	5.5	11
1579	35.6	1.25	0.96	0.8	2480	27.0±7.1	7.5	4.5
1711	35.6	1.25	0.96	0.9	1670	21.2±6.0	7	8.5
1914	35.6	1.25	0.96	0.9	1530	25.9±7.9	8	5.5
2106	21.4	1.25	0.93	0.9	460	19.7±7.3	8	6
561 No. 2	21.4	0.75	0.94	0.7	1500	15.4±4.1	6	4.5

[a] As an over-all check on the experiment and the analysis the point at 561 MeV/c was measured at the beginning and again at the end of the running. Both sets of data were measured independently by different scanners using two basically different measuring machines. The data was subjected to the same analysis procedure in particular with regard to the inelastic subtraction. The difference in the amount of inelastic background in the two runs is explained by the improved rejection during the later stages of scanning of false events simulating small opening-angle events.

forward direction. The chamber efficiency and resolution were obtained from a Monte Carlo calculation (M.C.) discussed in Sec. IV C.

III. FILM SCANNING AND ANALYSIS

Each trigger of the apparatus produced one photograph each of the beam and event chambers. Scanning and measuring of these photographs was done by professional film scanners on machines described in Ref. 9. Independently of the event-chamber photos, each beam-chamber photo was scanned for one and only one beam track. The frame numbers of events satisfying this condition were recorded in a log book. These one-beam-track events (1.B.T.) accounted for 60–80% of all photos, depending on the quality of the π^- beam for a given run. The event chamber photos of the 1.B.T. events were then scanned for two and only two showers. These two shower events accounted for 20–30% of the 1.B.T. pictures depending on the energy of the run. In addition, about 10% of the pictures had more than two showers or were completely blank. The remainder had only one shower.

All sets of photos with one beam track and two showers were measured relative to the Lucite grid fiducials, and the measurements were punched out automatically on IBM cards. These measurements were then processed by a 7094 computer program PIPPIN I. With data from additional measurements relating the Lucite grid fiducials to the internal fiducials together with measurements on beam tracks passing through both chambers to determine the relative alignment of the chambers, PIPPIN I could reconstruct the real space coordinates of the intersection of the beam track with the midplane of the H_2 target and the intersection of the showers with the midplane of their respective converters. These reconstructions do not depend on the π^- momentum, and the coordinates obtained from them are stored on magnetic tape for further analysis.

The spatial reconstruction required measurements for each event from a primary to several secondary fiducials. These measurements had to agree within preset limits to an accurate table of values. Rejections of events for which these measurements could not be found in the table served as a self-check on the day-to-day accuracy of the measurements.

PIPPIN I also checked to see that beam tracks were in a central $2\frac{1}{4}$-in.-diam spot in the H_2 target, and constructed a histogram of track positions in the target. The sparks from the tracks in the beam chamber left on the spark chamber plates a definite image (1.8 in. wide by 3.2 in. high) of the beam size at that point, and PIPPIN I checked that events were within it. In general, if an event was inside this region, it was also outside the allowed region of the H_2 target.

It is conceivable that due to different resolving times of the spark chambers, a beam track passing through the apparatus after an event triggers the logic but before the spark chambers fire could appear as the only track in the beam chamber and result in misinterpretation of the event. There were no thin plates directly preceding the first converter to detect such a straight through-charged particle. A check was made of the number of showers originating in the first converter versus the distance from the intersection point in this converter of the trajectory of the observed beam particle. This check and a check on the number of showers originating in each converter (both showers in the first, both in the second, or one shower in each) served to indicate that the rejection of two beam-track events effectively rejected pictures containing straight-through charged particles.

A closed expression for $\cos\theta_{\pi^0}$ in the lab can be obtained in terms of the positions of the γ-ray conversions, L and p_{π^-}. Since it is derived and discussed in Ref. 9 and is fairly complicated, it will not be given here. It has two important characteristics which introduce difficulties into the analysis: one, that it gives two solutions for the π^0 direction (corresponding to the lack of knowledge of which γ ray was most energetic); and two, if the opening angle of a measured event is below a given value, the solution is imaginary. To overcome the first difficulty it is necessary to compute the probability that each solution is the right one and assign a weight accordingly. In the limit of large statistics this procedure yields the correct π^0 angular distribution. The weight, however, depends on the π^0 direction. Hence, an iteration is required in which the angular distribution is assumed flat as a trial solution and the output distribution is fed back into the analysis until output and input agree. It takes about two iterations to obtain agreement. The second difficulty is overcome by computing the bisector of the γ-opening angle and taking that as an approximation to the π^0 direction. For all events the computed π^0 direction is used to determine a π^0 momentum and minimum-opening angle for the γ rays from a π^0 of that momentum. A histogram of number of events versus the ratio (observed γ-opening angle/calculated minimum-opening angle) can then be used to make a subtraction of 2γ events that are not elastic. The subtraction procedure is described in Sec. IV B.

Assumining all events to be elastic, a second 7094 computer program, PIPPIN II, calculated for each event the two $\cos\theta_{\pi^0}$ solutions, the γ-ray conversion efficiency, and the geometrical acceptance. Individual runs at the same momentum were analyzed separately and then all of these runs were combined. This procedure allowed a check for anomalies in a given run. None were found. The number of events versus $\cos\theta_{\pi^0}$ for each symmetric octant of the event chamber was computed to check for asymmetries in the chamber detection efficiency. None were found. No correction was needed for the detection efficiency of the C counter since the efficiency was measured to be better than 98.5% for straight through π^- and was therefore assumed to be 100% for the detection of at least one of two showers of an elastic event. No correction was made for the finite resolution in $\cos\theta_{\pi^0}$ since the Monte Carlo analysis of the experiment showed that equal numbers of events were exchanged between adjacent $\cos\theta_{\pi^0}$ intervals. Two-dimensional angular distributions versus $\cos\theta_{\pi^0}$ and φ_{π^0} (the γ-ray opening angle) were produced by PIPPIN II and used for further analysis.

IV. TREATMENT OF BACKGROUNDS

A. Target-Empty Effect

The first background taken into account was from events generated in the counters immediately fore and aft of the liquid H_2 target and in the Mylar windows of the target. This subtraction was done directly in PIPPIN II since at each energy both target-full and target-empty runs were taken. Target-empty trigger rates were about 15–25% of target-full rates. Consequently, $\frac{1}{3}$ of the running time was spent on target-empty runs. After scanning and analysis rejections in PIPPIN II, the target-empty background was closer to 10%. Furthermore, the target-empty data did not have the γ-opening angle distributions characteristic of elastic events. This is illustrated in Fig. 2.

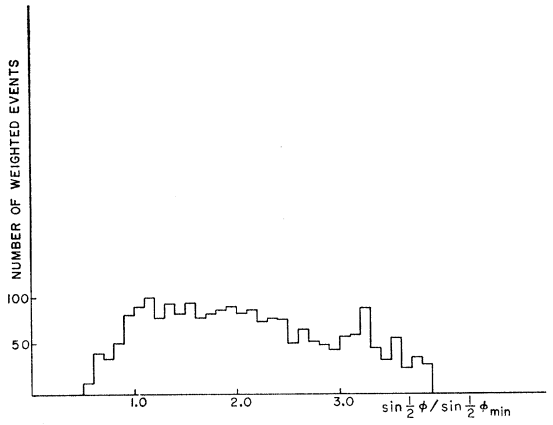

FIG. 2. γ-ray opening-angle distribution for target-empty run at 1434 MeV/c.

A straightforward computation of target-full minus target-empty data, including a corrected statistical error, was done by PIPPIN II, taking account of the difference in running times to collect the data.

B. Subtraction of Inelastic Events

Inelastic reactions (mostly $\pi^- p \rightarrow 2\pi^0 n$) are expected to contribute to the distributions of accepted events. Since no information about the neutron is obtained in this experiment, the one remaining tool for attempting to subtract any such background is the opening angle distribution between the two detected π^0 γ rays.

For the elastic charge exchange, the π^0 at a given $\cos\theta_{\pi^0}$ is monoenergetic and a simple relation for the fraction of π^0 decays with γ-ray opening angles between the minimum at that $\cos\theta_{\pi^0}$ and a given opening angle holds:

$$f = E_{\pi^0} p_{\pi^0}{}^{-1}(1-X^{-2})^{1/2},$$
$$X = (\sin\tfrac{1}{2}\phi)(\sin\tfrac{1}{2}\phi_{\min})^{-1}, \quad (1)$$

where ϕ is the opening angle and $\phi_{\min}$ is the minimum opening angle. It is seen that f is quite insensitive to the π^0 momentum p_{π^0} which enters only in the factor $(p_{\pi^0}{}^{-1}E_{\pi^0})$. It is therefore convenient to plot opening angle distributions as a function of X. Furthermore, Eq. (1) shows that the main effect on f of the resolution of the apparatus comes from X and to first order

$$f' = E_{\pi^0} p_{\pi^0}{}^{-1}[1-(X+a)^{-2}]^{1/2},$$

where a can be considered an adjustable parameter. For perfect resolution $a=0$ and if $X=1$, $f=0$. If $a\neq 0$, however, $f'\neq 0$, which results in measured opening angles less than the kinematically allowed minimum.

The Monte Carlo calculation (M.C.) indicates at all momenta that 60% of the elastic data are contained between $X=0.9$ and $X=1.25$. Furthermore, the M.C. shows that for the target length 2.22 in., and measuring uncertainties in the spark chamber $\lesssim\pm 0.5$ in., a is $\approx 0.3\pm 0.1$, in order to get agreement between the experimental and M.C. opening angle distributions for $X<1.25$. Therefore, for $X>1.25$, f' is quite insensitive to the allowed variation in a.

Because of the fact that above opening angles containing 60% of the elastic π^0 decays we begin getting events with detection efficiency $<10\%$, it is convenient to cut the data in an interval $0.9\leq X\leq 1.25$. If we compare the experimental opening-angle distributions with the results of the M.C. for various assumed measuring accuracies, using a Gaussian distribution with variable width, there is a width which will give good agreement between the two distributions in the stated interval. This could be done at all momenta for half widths of 0.2–0.4 in., which was entirely consistent with estimated measuring accuracies. The primary effect of changing the width is simply to change the number of events in the X intervals 0.9–1.0 and 1.1–1.25 relative to the number of events in the interval 1.0–1.1. The tail of the distribution ($X>1.25$) remains essentially unchanged.

Below $X=0.9$ in the experimental distributions there is a background plateau, due in part to the inelastic events for which the γ rays are from different π^0's and the opening angle between them is less than the kinematically allowed limit of an elastic π^0 with direction along the bisector of the two γ rays. Above $X=1.25$ the elastic tail falls so rapidly compared to the experimental distribution[11] that the following procedure was adopted for making the inelastic subtraction. The M.C. results were normalized to the number of experimental events for $0.9\leq X\leq 1.25$ and the elastic tail for $X>1.25$ as given by the M.C. was subtracted from the experimental distributions. Corrections for any elastic events for $0.8\leq X\leq 0.9$ were also made. A smooth extrapolation was then made between the plateau and the remaining events above $X=1.25$ to give an estimate of the number of inelastic events in the region of accepted elastics. The elastic M.C. results were then renormalized to the corrected number of experimental events between $X=0.9$ and 1.25 and the procedure repeated. Some of the results are shown in Fig. 3.

Attempts were made to fit the inelastic background with a M.C. simulation of the experiment for the case $\pi^-p\rightarrow 2\pi^0 n$ using phase space to govern the final-state distributions. Below 1434 MeV/c the inelastic M.C. failed to fit the experimental background. At 1434 MeV/c and above, the fits were fairly good, although there was a slight excess of experimental background events at small opening angles ($X<1.0$).

The inelastic M.C. was done with and without the anti system, and with and without a chance of detecting the neutron. The over-all rates for these cases were quite different, but the opening-angle distributions did not change significantly. Below 1434 MeV/c an isobar model[12] might give better results, but this has not been tried.

A study of photographs was made for events with small opening angles to determine whether or not the excess of events was due to a stray beam particle traversing the apparatus. There was no indication of this, as mentioned earlier, but there were indications that the excess is due to either of two causes: a single wide-angle shower from which one of the electrons backscatters in the second converter or the rear $\frac{3}{4}$-in. Al wall of the chamber box; or a neutron star which produces a wide-angle secondary that backscatters. The reduced spark-chamber efficiency for wide-angle tracks (in the presence of additional small-angle tracks) can result in a weak track that is missed in the scanning. The original γ-ray conversion (or neutron star) with the backscattered track some distance away is then mistaken for a two-shower event.

In any case, it is unlikely that successful fits to the background will result in an amount of background appreciably different from that already determined by the procedure described above. The amount and uncertainty in this background (Table I) is $\sim(20\pm 5)\%$ depending on the beam momentum. This uncertainty is the largest single cause of uncertainty in the values obtained for the forward amplitude.

C. Monte Carlo Analysis and Determination of Absolute π^- Momentum

The problem of getting a good fit between the elastic M.C. and the experimental opening-angle distributions is closely related to the question of absolute π^- momentum p_{π^-}, due to the sensitivity of the experimental distributions to p_{π^-}. A shift of $\pm 2\%$ from the momenta in Table II produces opening-angle distributions which are generally inconsistent with the M.C. results.

The M.C. is an exact reproduction of the experiment to the extent that it produces π^0 decays generated according to phase space from π^-p interactions occurring randomly along the H_2 target with appropriate variations in π^- momentum. The coordinates of the γ rays produced are subjected to a random distribution of

[11] Since all events are treated as elastic events by PIPPIN II, the inelastic events at wide opening angles are given an excessive weight which keeps the tail of the γ-ray opening-angle distributions from falling as rapidly as it would were inelastic events weighted correctly.

[12] M. Olsson and G. B. Yodh, University of Maryland Tech. Report No. 358, 1964 (unpublished); J. D. Oliver, I. Nadelhaft, and G. B. Yodh, Phys. Rev. **147**, 932 (1966).

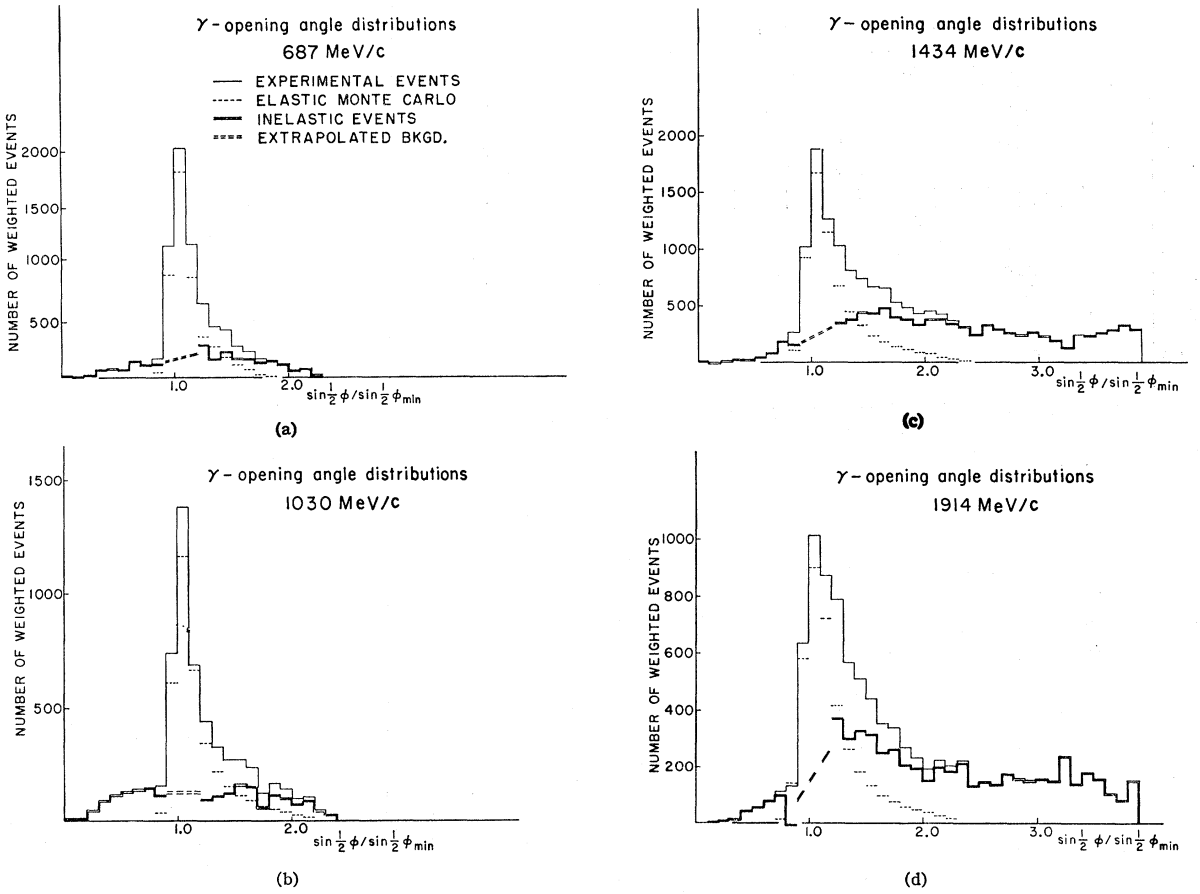

FIG. 3. (a)–(d) γ-ray opening-angle distributions for 687, 1030, 1434, and 1914 MeV/c, determined by the procedure described in Sec. IV C. The 687-, 1030-, and 1434-MeV/c fits are typical. The 1914-MeV/c fit was the least satisfactory of all the data.

variations representing measuring errors. The event is then reconstructed in the same way PIPPIN II reconstructs experimental events. After extensive M.C. studies of the effect of various distributions in $\Delta p/p$ and in the measuring errors, it was concluded that the experimental opening-angle distributions when compared with the M.C. results offer a sensitive check on the assumed π^- momentum.

The values of p_{π^-} used in the initial analysis were those obtained from the wire orbit results corrected for energy loss of the beam in material between B.M. II and the midpoint of the H_2 target. As mentioned in Sec. II A the current in B.M. I was changed from the wire-orbit values to maximize the count rate in T_4', but no check was made to determine the effect of this on the beam momentum at the H_2 target. In the later stages of analysis it became apparent that the data from 930–1427 MeV/c fit the M.C. opening-angle distributions quite well. However, the 575–810-MeV/c data indicated that the value of the π^- momentum should be reduced 2% and the data above 1423 MeV/c indicated that p_{π^-} should be increased 1% to obtain the best agreement with the M.C. results.

To investigate this point further, an evaluation was made of the time of flight measurements on π's, and d's (Sec. II A). The differences in times of flight between π's and p's and between p's and d's were measured for flight paths between two pairs of counters (S1-S2 and S1-S3; the counters S1, S2, S3 were located at approximately the same positions as T_1, T_2, T_3). The beam momentum was computed from these differences taking into account energy losses of the beam in the material between the counters and shifts in the observed π time due to the μ's and e's in the beam. The results showed deviations from the wire orbit results of the same magnitude and direction as the shifts needed to bring the experimental and M.C. distributions into agreement. Fig 4 shows the extent of the disagreement among the values of p_{π^-} arrived at by the different methods. Figure 5 shows the effect on the opening-angle distribution at 687 MeV/c of a 2% upward shift in the value of p_{π^-} used to get the 702-MeV/c distribution in Fig. 3. Further studies of the opening-angle distributions showed that shifts up to $\pm 1\%$ from the values in Table II would yield distributions that still give reasonable agreement with the M.C. results. By taking this into account with the size of the discrepancies among the different measurements of p_{π^-}, an esti-

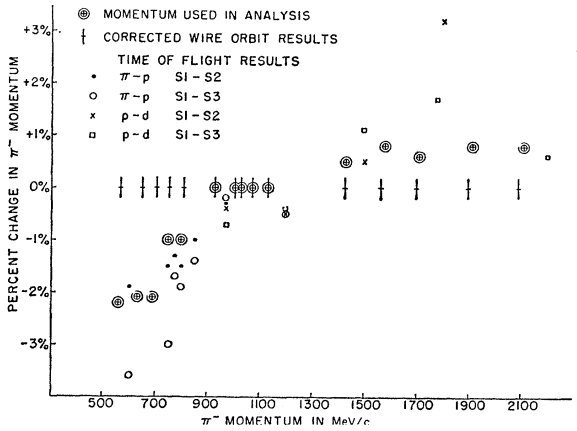

FIG. 4. Spread in the absolute value of the π^- momentum for the different methods of measurement compared to the corrected wire-orbit measurements.

mate was made at each momentum of a possible systematic error (δp_π-) in p_π-. The resulting increase in the uncertainty of the forward amplitude is about twice δp_π-(i.e.,$\pm 2\%$).

D. μ and e Contamination of π^- Beam

As mentioned in Sec. II A, the μ and e components of the negative beam were measured with a gas Čerenkov counter. The short beam (60 ft from internal machine target to the H_2 target) gave rise to a relatively small μ contamination. A typical Čerenkov curve showing (T1,T2,T3,T4,$\check{C}$) coinc./(T1,T2,T3,T4) coinc. in percent versus pressure in the Čerenkov counter is shown in Fig. 6. These curves plateau at high pressure at 100%, but only the lower portion of the curve is shown in Fig. 6 to illustrate the detail of it. Referring to Fig. 6, the points P_μ and P_π are the thresholds for the detection of 750 MeV/c μ's and π's. Since there is a spread in momentum of the particles, μ's and π's are assumed to be detected beginning at P1 and P3 respectively. P2 is normally assumed to be the point at which μ_1's, μ's originating in the internal target and due to π^- decay along the beam before B.M. I, are collected with full efficiency. The rise from P2 to P3 is assumed to be the contribution of knock-on electrons produced in the Čerenkov counter and the collection of μ_2's. μ_2's come from π^- decays after B.M. II and have a broader momentum distribution than the μ_1's,

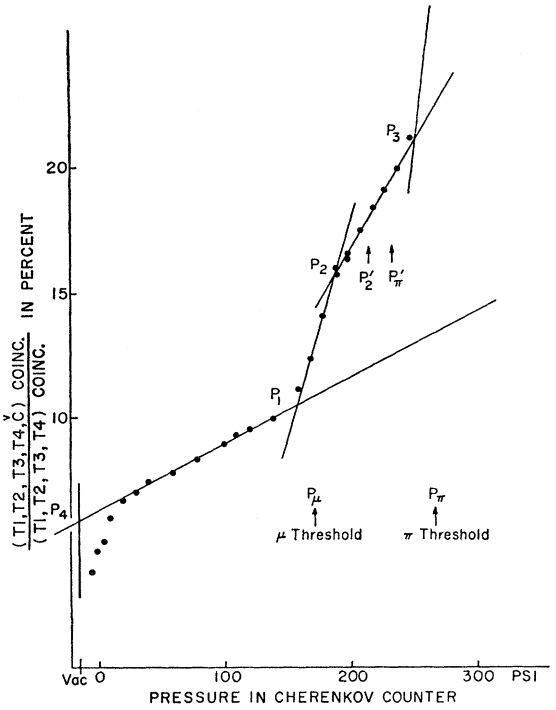

FIG. 6. Čerenkov-counter curve for 750-MeV/c π^- beam.

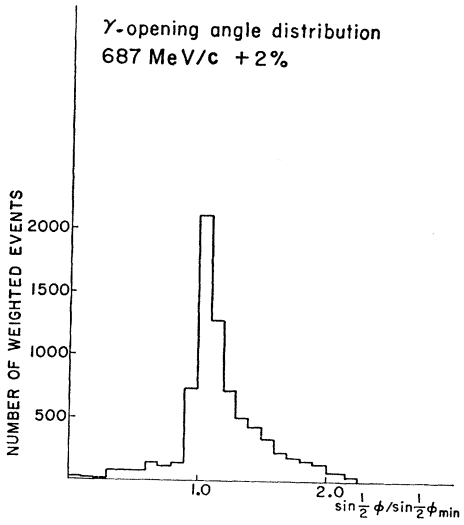

FIG. 5. γ-ray opening-angle distribution for 687 MeV/c data with a +2% shift in π^- momentum. The depletion of events in the interval x=0.9–1.0 is characteristic of an upward shift in momentum.

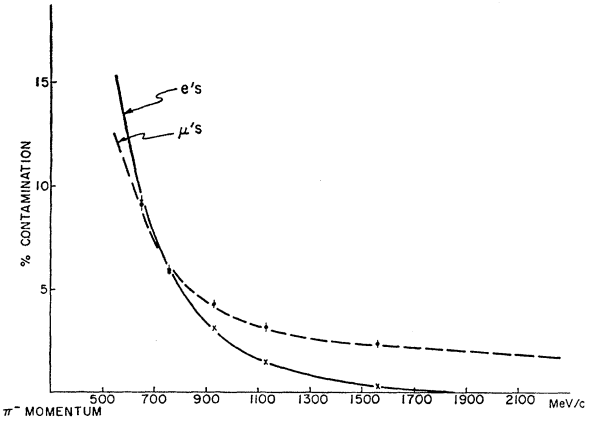

FIG. 7. μ and e contamination of π^- beam determined from Čerenkov-counter measurements.

which have to pass through B.M. II. The effect of the knock-on electrons is determined by the line P4-P1. P4, in fact, gives the electron contamination. However, the rise from P2 to P3, after correcting for the continuing rise from P4 to P1 is too big to be explained by μ_2's alone, the amount of which can be calculated directly. The point P_π' is the threshold for a π with momentum 10% less than 750 MeV/c, so that a contamination of a few percent of π's differing in momentum up to 10% of p_{π^-} could explain the excess rise. P_2 indicates the maximum contribution of u_2's. Uncertainties in the actual amount of these contaminations comes from the uncertainties in fitting straight lines to the Čerenkov curve over the appropriate intervals. The results are indicated in Fig. 7.

V. MISCELLANEOUS CORRECTIONS AND UNCERTAINTIES

The forward amplitude $d\sigma/d\Omega(0°)$ in terms of the extrapolated number of weighted events per unit solid angle $\Delta n/\Delta\Omega(0°)$ is given by

$$\frac{d\sigma}{d\Omega}(0°)=\left(\frac{\Delta n}{\Delta\Omega}(0°)\right)_{H_2}\left(\frac{1}{\text{effective No. of }\pi^- \text{ in.}}\right)\times\left(\frac{1}{\text{No. of nuclei/cm}^2}\right). \quad (2)$$

$[\Delta n/\Delta\Omega(0°)]_{H_2}$ has been corrected for the target-empty effect. Since the film scanning accepted only events for which there was only one beam track in the beam chamber, for each run:

effective No. of π^- in.

= (No. of pictures with one beam track/ total No. of pictures) × (No. of π^- to get all pictures).

Most of the variables in the above expressions are

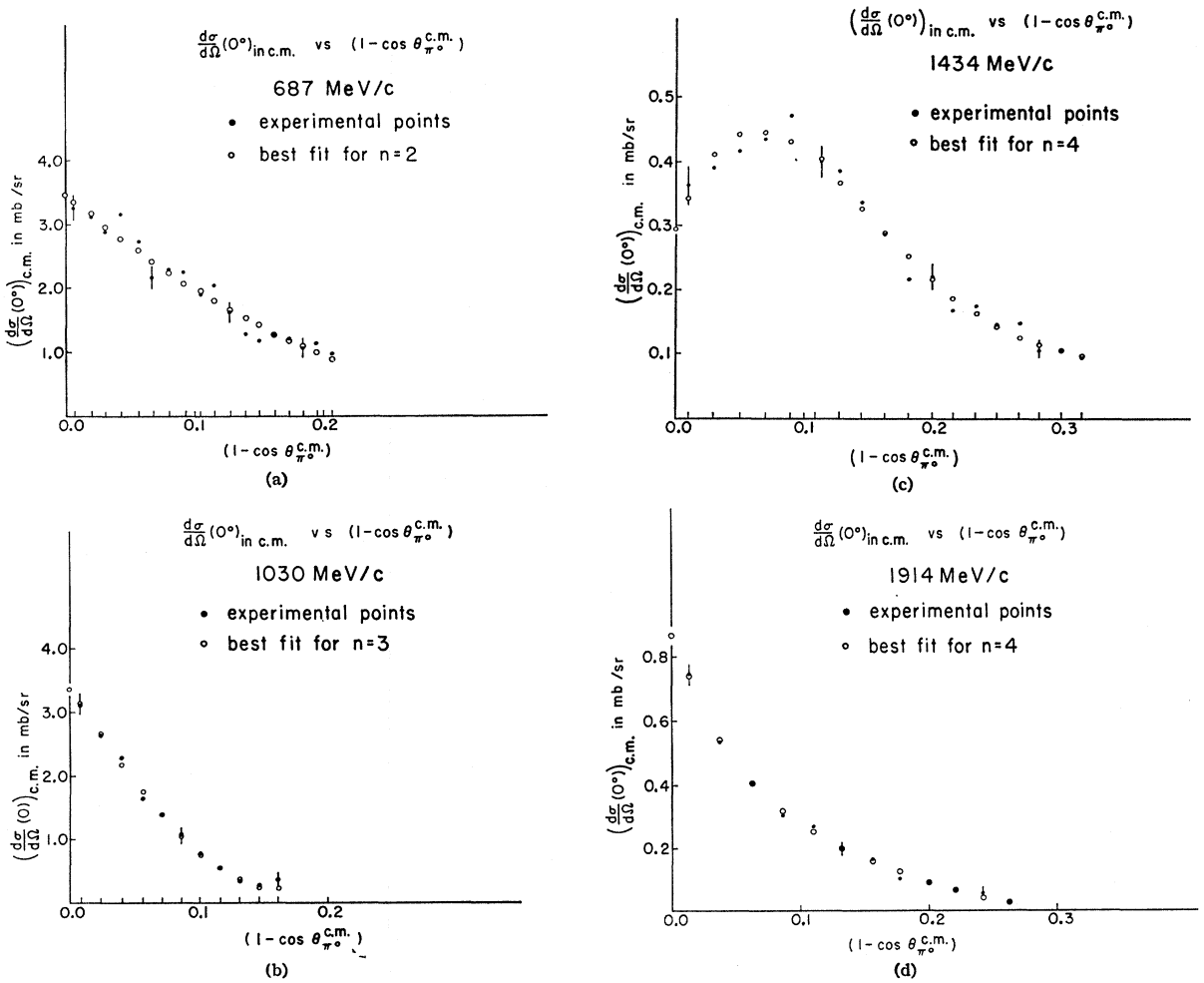

FIG. 8. (a)–(d) Angular distributions for $\pi^- p \to \pi^0 n$ for π^- momentum indicated, without inelastics subtracted. The open circles are the best fits for $n=2$ at 687 MeV/c, $n=3$ at 1030 MeV/c, and $n=4$ at 1434 and 1914 MeV/c. The errors on the experimental points are the statistical errors only.

subject to corrections, some of which add systematic uncertainties to the result.

(A) Δn, the weighted number of events in a $\cos\theta_{\pi^0}$ interval, in addition to the corrections for target-empty effect and inelastic backgrounds is affected by the following factors:

(1) Scanner inefficiencies. These varied between 2.2 and 8.3% with uncertainties $\sim\pm 1.5\%$.
(2) Events lost because of improper measuring or faults in card punching.
(3) A 6% antimony content in the lead converters. This requires a correction of $+5\%$ to the conversion efficiency for 2γ events relative to the efficiency of pure lead.
(4) Dalitz decay mode of the π^0. 1.2% of the π^0's decay via the mode $\pi \rightarrow e^+e^-\gamma$, which will not be accepted by the apparatus.
(5) The fraction of events in the accepted γ opening angle interval. This fraction was nominally 60%, but several factors affecting the M.C. determination of it produce an uncertainty of about $\pm 1\%$.
(6) Values of the γ-conversion efficiency. The values used by PIPPIN II were determined from the Berkeley tables[13] of pair-production cross sections and were generally 5% higher than values determined from the calculated cross sections of Malamud.[14] Hence Δn was increased by $2\frac{1}{2}\%$ and an additional uncertainty of $\pm 2\frac{1}{2}\%$ was included in the final error.
(7) The loss of events due to detection of the elastic neutron in the antisystem. This was estimated at 1%.

(B) The effective number of π^- in must be corrected for a number of effects in addition to the μ and e contamination:

(1) The fraction of beam tracks outside the allowed 2.2-in. central beam spot of the hydrogen target. This effect combined with the loss in Δn due to (A.2) varies between 1.2 and 7.5% depending on momentum.
(2) π^- decays between the last telescope counter and the midpoint of the hydrogen target. This number varies between 0.3 and 2.0% depending on beam momentum and telescope-to-target distance.
(3) The fraction of π^- contained in the same rf bunch. This fraction was determined to be about 0.5% by counting the fraction of π^- in adjacent rf bunches. Since the telescope could count up to 50 Mc/sec, it missed only extra π^- in the same rf bunch.

(C) The number of nuclei/cm^2 was subject to the following corrections:

(1) Curvature of the hydrogen-target flask. Averaging over the allowed 2.2-in. central spot gave an effective target length of 2.22 in.
(2) Boiling of the liquid hydrogen. The percentage of gaseous hydrogen in the full flask was estimated at 1% from photographs of the hydrogen boiling in the flask.
(3) Residual gas in the flask during target-empty runs. This effect was estimated at 2% by using Boyle's law and results in a 2% loss of events when the target-empty subtraction is made.

The over-all uncertainty due to these effects, excluding the target-empty effect is given in col. 8 of Table I. The statistical uncertainty, which is given in the next section is approximately doubled due to the target-empty subtraction.

VI. EXTRAPOLATION TO ZERO DEGREES AND COMPARISON WITH THE DISPERSION RELATIONS

In order to determine $\Delta n/\Delta\Omega(0°)$ which appears in Eq. (2), the angular distributions of weighted events versus $\cos\theta_{\pi^0}$ are extrapolated to zero degrees. Since the quantity of the data was not enough to do the inelastic subtraction for each $\cos\theta_{\pi^0}$ bin, the extrapolation was done without subtracting the inelastic data. $\Delta n/\Delta\Omega(0°)$ was then corrected for the amount of background determined in Sec. IV B. The uncertainty in the forward amplitude due to subtracting the integrated inelastic background was estimated to be small relative to other errors in the experiment. To produce a sizable effect, the inelastic angular distribution would have to deviate considerably from a constant percentage of the total data in each angular bin. A visual inspection of the opening-angle distributions for each bin indicated that this might be the case only at the largest angles, which have a small effect on the extrapolation to zero degrees.

The angular distributions were fitted with polynomials in $(\cos\theta_{\pi^0})$ up to order $n=5$. The bin widths used were 0.005 and 0.010 in $\cos\theta$. Results for the two cases were consistent, but fits using the smaller bin width were generally stable over a larger interval in n and were therefore preferred. Linear fits were possible for the lowest momenta, but above 802 MeV/c, $n=2$ was the lowest-order fit that gave acceptable values of χ^2. In general, there is an interval $n_1 \leq n \leq n_2$ for which both $\Delta n/\Delta\Omega(0°)$ and L were relatively constant. $L^2=\chi^2$/degree of freedom. Fits for values of L between 0.7 and 1.5 have between 90% and 10% confidence levels.

Table II summarizes the results of the experiment. The number of experimental points for each angular distribution is given in col. 2 of Table II. $\Delta n/\Delta\Omega(0°)$ was taken as the mean of values for $\Delta n/\Delta\Omega(0°)$ between n_1 and n_2.

The resulting forward amplitudes and their uncertainties are given in col. 3 of Table II. The uncertainty is due to the combined uncertainties in cols. 8 and 9 of Table I. All individual uncertainties are assumed Gaussian distributed and are combined in quadrature. The uncertainty in col. 9 is the quadrature of the fitting

[13] High-Energy Particle Data, University of California Radiation Laboratories Report No. UCRL-2426 (unpublished).
[14] E. Malamud, Phys. Rev. **115**, 687 (1959).

TABLE II. Summary of the results of various fits to the angular distributions. Col. 1, incident π^- momentum. Col. 2, No. of points in fit. For polynomial fit. Col. 3, $(d\sigma/d\Omega)(0°)$ and total uncertainty in mb/sr. Col. 4, orders of fit n_1–n_2. Col. 5, $\bar{L}=\langle[\chi^2/(\text{degree of freedom})]^{1/2}\rangle_{\text{av}}$. Col. 6, slope of $(d\sigma/d\Omega)(0°)$ and its variation over the fit interval n_1–n_2, in (mb/sr)/$\Delta\cos\theta$. For exponential fit. Col. 7, $(d\sigma/d\Omega)(0°)$ in mb/sr. Col. 8, $L=[\chi^2/(\text{degree of freedom})]^{1/2}$. Col. 9, slope of $d\sigma/d\Omega(0°)$ in (mb/sr)/$\Delta\cos\theta$.

1	2	3	4	5	6	7	8	9
561 No. 1[a]	18	3.28±0.26	1–5	0.66	18±7	3.61	0.58	26
636	18	2.95±0.22	1–3	0.86	13±2	3.35	1.06	25
687	18	3.38±0.24	1–5	1.04	12±5	4.02	1.20	28
750	18	2.48±0.20	1–5	0.62	13±7	2.77	0.56	18
802	18	1.33±0.10	1–5	1.05	6±3	1.59	1.06	10
930	11	2.42±0.15	2–4	1.06	32±1	2.60	1.01	45
1005	11	3.15±0.24	2–4	1.01	41±7	3.32	0.86	49
1030	11	3.43±0.22	2–4	0.58	34±4	3.90	1.10	61
1077	18	1.70±0.10	2–4	0.69	12±1	2.10	1.20	23
1134	11	1.04±0.07	2–5	0.75	12±1	1.18	1.08	18
1434	18	0.31±0.04	3–5	1.03	−4±2	not fitted with exponential		
1529	12	0.56±0.05	2–5	0.56	55±2	0.63	1.02	6
1711	12	0.73±0.08	2–5	1.22	10±5	0.73	1.13	7
1914	12	0.87±0.09	3–5	0.71	11±3	0.95	1.05	11
2106	18	0.56±0.06	3–5	0.81	6±1	0.58	0.94	7
561 No. 2	18	3.42±0.26	1–3	0.85	19+5	3.80	0.79	31

[a] As an over-all check on the experiment and the analysis the point at 561 MeV/c was measured at the beginning and again at the end of the running. Both sets of data were measured independently by different scanners using two basically different measuring machines. The data was subjected to the same analysis procedure in particular with regard to the inelastic subtraction. The difference in the amount of inelastic background in the two runs is explained by the improved rejection during the later stages of scanning of false events simulating small opening-angle events.

uncertainty, the statistical uncertainty, and the uncertainty resulting from the ±1% π^- momentum error δp_{π^-} discussed in Sec. IV C. The first of these uncertainties is obtained from the extreme values of $\Delta n/\Delta\Omega(0°)$ for fits between n_1 and n_2 and was found to vary between 1 and 10%. The statistical uncertainty of a given fit was determined to be ~3%. From the analysis of the data assuming a few percent shift in the π^- momentum, it was found that $\delta p_{\pi^-}=\pm 1\%$ gives rise to a ±2% uncertainty in $\Delta n/\Delta\Omega(0°)$. This latter error could have been reduced by accepting more than 60% of the elastic data in the γ-ray opening-angle analysis, but this gain is offset by the rapid rise of inelastic background above the 60% cutoff. Columns 4 and 5 of Table II give for each momentum the range of accepted fits n_1–n_2 as well as $\bar{L}$. $\bar{L}$ is the mean value of L in the range n_1–n_2. The slope of $d\sigma/d\Omega(0°)$ and its variation over n_1–n_2 is given in col. 6 of Table II.

Excluding the 1434 MeV/c point, exponential fits of the form $Ae^{-B(1-\cos\theta_{\pi^0})}$ were also made, with A and B varied independently to obtain a best fit. Because L is generally closer to 1 for the exponential fits, they are statistically better than the polynomial fits. This is quite surprising at the low momenta where the total angular distribution measurements[4] indicate that the number of contributing partial waves is ~3. An exponential fit is usually associated with a diffraction peak, where a large number of partial waves contribute. The exponential fits, as might be expected, give systematically higher values of $d\sigma/d\Omega(0°)$, by up to 25%. The value of $d\sigma/d\Omega(0°)$ and its slope ($A\times B$) for these fits is included in Table II, but the polynomial fits are preferred at the low momenta since physically they are more reasonable.

The results of the polynomial fits are plotted in Fig. 9, along with the results of previous experiments and the dispersion-relation calculation of Höhler. This experiment is in general agreement with these other results. However, in spite of significantly greater statistics in this experiment, col. 6 of Table I, the systematic effects discussed above limit its over-all accuracy. However, even with these effects taken into account, there are small deviations observable in making a comparison with the dispersion relations. In the region 600–700 MeV/c, the present results are low while in the region 1400–2100 MeV/c they are high.

It is possible that part of the discrepancy between the results of this experiment and the dispersion relations is due to the uncertainty in the dispersion-relation calculation itself, since the calculation depends on experimental values of the total elastic cross sections. The size of these effects is estimated and discussed in the paper of Amblard *et al.* (Ref. 5) and in Ref. 7 and does not completely account for the discrepancy.

While it is conceivable that any one of the larger effects in the present experiment has been incorrectly taken into account (e.g., μ and e background and inelastic background), on the basis of the discussions given we do not believe this to be the case beyond the quoted errors. For example, to bring the lower energy points into agreement, the determination of the inelastic background at 561 and 636 MeV/c would have to be a factor of 2 too high, or alternatively the determination of the combined μ and e contamination would have to be a factor of 2 too low. Furthermore, to bring all of the data into agreement requires (a) raising the low-energy values, (b) leaving the middle-energy values unchanged, and (c) lowering the high-energy values.

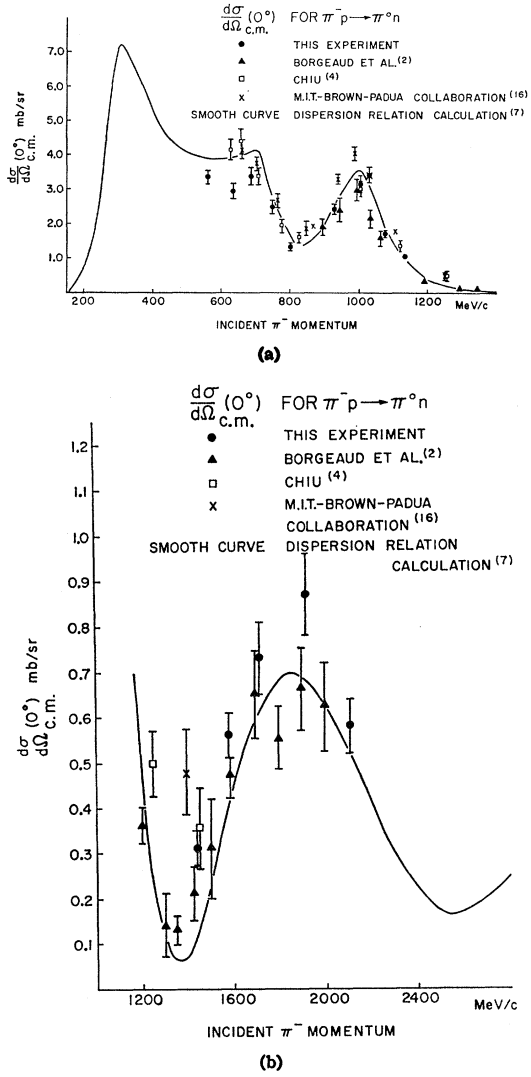

FIG. 9. (a), (b) Comparison of the values of $d\sigma/d\Omega(0°)$ from this experiment with the results of other experiments. The smooth curve is the dispersion calculation of Ref. 7.

Even with the relatively large errors on some of the systematic effects in the experiment, there is no way in which some combination of them could combine to bring about the above changes.

One interesting characteristic of the exponential fits is that excepting the 650-MeV/c point which is too low and the 1030 MeV/c point which is too high, the remaining points up through 1130 MeV/c are in almost perfect agreement with the dispersion relation. This result, however, is considered fortuitous. Above 1427 MeV/c, the exponential fits give up to 10% higher values of $d\sigma/d\Omega(0°)$ than the polynomial fits.

In conclusion, the results of this experiment, with higher statistics than those of previous experiments,[2,4,15] are in general agreement with earlier work but do not resolve the nature of the existing discrepancies between the experimental and theoretical results.

ACKNOWLEDGMENTS

The author would like to thank his Ph.D. thesis advisor, Professor G. T. Reynolds, for many helpful discussions throughout the course of this experiment. The equipment was built at the Elementary Particles Laboratory with the aid of the shop staff. Special thanks are due Paul Botos and Edward Kleckner for their assistance in the construction and testing of the equipment and running of the experiment. Paul Kunz also helped in the running. Edward Kleckner did much of the initial programming for the experiment. Grateful acknowledgements are due the excellent scanning staff of the laboratory, in particular to Mrs. Marion Hoffmann who helped with the laborious bookkeeping of the daily computer work. The author wishes to thank Professor Milton White and the Princeton-Pennsylvania Accelerator staff for their hospitality and assistance during the running of the experiment, and Professor A. Berthelot for his hospitality at C.E.N. Saclay, where some of the early analysis was carried out. Dr. René Turlay advised on the wire orbit calibration of the beam and Dr. A. J. S. Smith performed the time-of-flight measurements. Discussions with Dr. Peter Sonderegger were most helpful in directing the course of the analysis and in making a comparison with the Saclay experimental results. Finally, thanks are due all of the graduate students at the laboratory who advised and assisted at various times throughout the experiment.

[15] The author wishes to thank Professor R. E. Lanou of Brown University for providing more recent results than those of Guerriero in Ref. 4.